SILENT NIGHT SURVEILLANT

DESIGNED BY:
BRIAN SPINELLI, CHRIS MCCORMICK, AND HENRY JONES

UCLA MAE 154A FINAL REPORT WINTER 2025

Table of Contents

I. Mission Description

1. Motivation

Every year, Santa Claus and his elves are tasked with evaluating the character of every person on this Earth, to be entered on his naughty or nice lists. In past years, this has been a trivial feat for Santa and has posed no issues. However, as the population continues to grow, Santa is struggling to keep up. If he is not careful, he might not finish in time for Christmas. He needs help.

Santa has recruited only the top engineers to design him a surveillance UAV to conduct a covert, naughty-nice assessment of the UCLA student body. The appropriately named Silent Night Surveillant (SNS) UAV will be launched from the offshore Christmas Carrier, fly to UCLA, locate a student of interest, surveil the student for 24 hours, and return to the ship for data processing and transmission back to the North Pole.

Fig. 1 Santa analyzing recorded SNS UCLA data

2. Mission Requirements

The mission requirements set for the SNS ensure optimal surveillance capability and performance to meet Santa's needs. Set flight requirements are detailed below.

Minimum Endurance	24 hours
Maximum Stall Speed	90 fps
Minimum Top Speed	161.3 fps
Minimum Max Climb Angle	23 degrees
Minimum Max Service Ceiling	10,000 ft

Table 1 Flight mission requirements

The SNS must also be capable of circling a person moving at a walking pace and carrier operations. A catapult launch system will be equipped on the Christmas Carrier along with an arresting wire the SNS can catch with a tail hook for landing.

3. Payload

To adequately conduct high-level surveillance for Santa, the Surveillance Series S512 Camera was chosen as a payload for the SNS. Weighing a total of 50 lbs and equipped with thermal imaging and infrared sensors, this camera provides a lightweight and advanced solution to aerial surveillance.

Manufactured by Gyro-Stabilized Systems, the S512 Camera has a gimbal 5-axis stabilization system to ensure stable imaging and tracking no matter the aircraft's attitude or land geography. An equipped tracking system can "track on moving and non-moving objects in a wide range of applications" to meet all of Santa's needs.

Fig. 2 Surveillance Series S512 camera payload

The camera was also selected for the SNS due to its 240x zoom capability, resulting in a 59.3 ft FOV from 10,000 ft or 296.5 ft FOV from 50,000 ft. This allows for a versatile cruise altitude for surveillance depending on weather conditions or level of stealth desires.

II. Aircraft Details

1. Sizing and CAD

A CAD model was created to visualize the SNS design. The renderings of Figure 3 show the SNS flying over Los Angeles. In the right image, you can see the camera payload protruding from the underside of the fuselage. Figure 4 shows the technical drawings of the aircraft from a front, top, side, and isometric view. In these drawings, you can see the retractable landing gear and tail hook extended.

Fig. 3a & 3b Final aircraft renderings

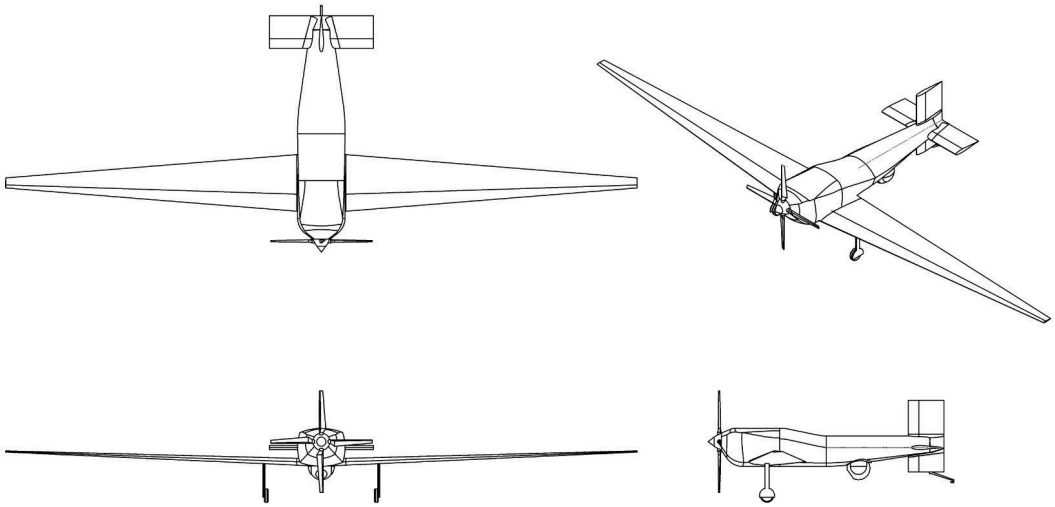

Fig. 4 Design drawings

2. Aircraft Specifications

The dimensions and general specifications of the aircraft can be seen in Table 2. Note that "x" variables are measurements from the nose of the aircraft to the center of mass of the object referred to in the subscript. For instance, x_{eng} refers to the distance of the engine's center of mass from the nose of the aircraft. Key elements of the design which are reflected in Table 2 include its high aspect ratio, high wing area, and payload position.

Wing	Values	Horizontal Tail	Values	Vertical Tail	Values	Fuselage & Miscellaneous	Values
b	27.9 ft	b	4.61 ft	b	3.16 ft	$length$	10.44 ft
$\bar{c}$	1.56 ft	$\bar{c}$	1.44 ft	$\bar{c}$	1.58 ft	h_n	0.63
c_r	2.67 ft	-	-	-	-	h_{cg}	0.41
c_t	0.44 ft	-	-	-	-	SM	0.22
S	43.5 ft^2	S	6.63 ft^2	S	5.01 ft^2	x_{eng}	2 ft
AR	17.9	AR	3.21	AR	2.00	x_{pl}	6.66 ft
λ	0	λ	0	λ	0	W_{dry}	376 lbs
Λ	0.17	Λ	0	Λ	0	W_{wet}	425 lbs

Table 2 Aircraft specifications

For the airfoil selection, the NACA 2412 was chosen for the wings. This cambered airfoil was picked due to a high maximum 2-D lift coefficient of around 1.5 at our cruise Reynolds number. The NACA 2412 also has a high stall angle of attack of approximately 15 degrees, which is beneficial for a low stall speed. For the tail, the symmetric NACA 0012 was chosen. Due to an incidence angle of 2.6 degrees, the symmetric airfoil provided sufficient downlift to keep the aircraft in trim conditions.

The weight breakdown of the aircraft is presented in Figure 5. These weights were determined using the Niccolai equations. A key observation made toward the end of the design process is that the Niccolai equations tend to overestimate the weight of control surfaces in smaller aircraft. Initially, when the aircraft was larger, this inaccuracy was not apparent. However, as the aircraft was optimized and became lighter, the discrepancy became more pronounced. Ultimately, the Niccolai equations estimate that the control surfaces weigh more than the entire fuselage, which is unrealistic. Since this inaccuracy was not identified until the optimization was complete, there was no opportunity to address it.

An important observation that can be made from Figure 5 is that most of the weight of the aircraft comes from its engine. This was not initially the case before optimization when the wing made the dominating weight contribution. As optimization continued, the structural weight of the aircraft progressively lessened, leaving the engine as the heaviest portion of the plane.

This indicates that for further optimization, using a lighter engine would be preferable if one can be found with appropriate power. This will be discussed in more detail later.

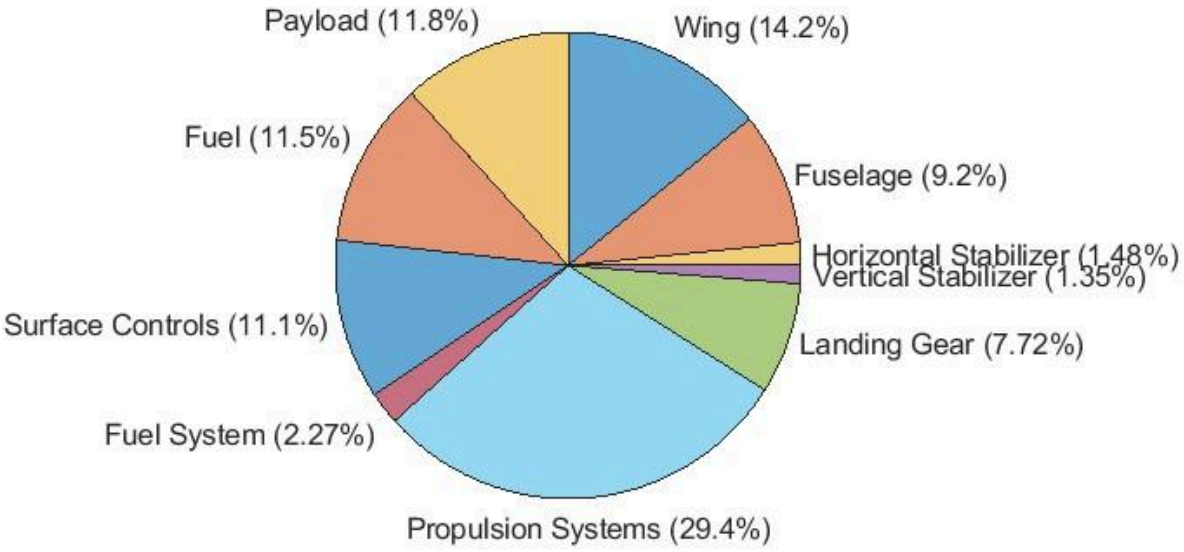

Fig. 5 Weight breakdown of SNS UAV

3. Aircraft Configuration

The driving forces that guided the aircraft configuration to its current state are minimizing weight and ensuring mission functionality. Every design decision was evaluated through these two considerations before reaching a determination. A prime example of this design strategy is the wing position. A low-wing configuration reduces weight in two ways. First, it allows for a continuous wing spar to pass uninterrupted beneath the engine. If a mid-wing configuration were chosen, the wing spar would be interrupted by the engine, requiring a heavier structure to maintain the same level of structural integrity. Additionally, the low wing enables the use of shorter, lighter landing gear. In contrast, a high-wing configuration would necessitate longer, heavier landing gear. This choice also aligns with the aircraft's mission, which includes takeoff and landing from an aircraft carrier. Sturdy landing gear is crucial for such operations, making the low-wing configuration the logical choice.

Another aspect of the SNS configuration that warrants discussion is the position of the vertical tail. It was decided to position the vertical stabilizer such that a portion of its area extended below the fuselage. This limits unintended rolling moments due to rudder deflection,

creating more predictable handling and benefiting the SNS as a camera platform. Furthermore, it provides a convenient low mounting point for the tail hook and tail wheel, while also creating additional clearance for the camera when the aircraft is on the ground.

4. Propulsion

Two engines, the Rotax 912 and 914, were included in the SNS's optimization efforts. The Rotax 914 is the heavier and more powerful option, but the lighter engine, the 912, was ultimately selected. The specifications for both engines are below.

	Rotax 912	Rotax 914
	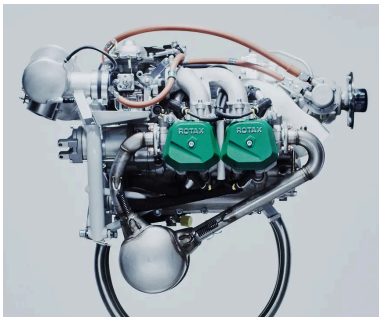	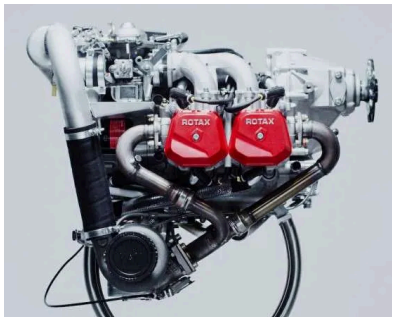
Power	78 *hp*	100 *hp*
Specific Fuel Consumption	0.386 *lbs/shp/hr*	0.386 *lbs/shp/hr*
Weight	125 *lbs*	164 *lbs*
Cruise RPM	5500	5500
Gearbox Ratio	2.27:1	2.43:1

Table 3 Engine specifications

Propeller analysis for each engine was performed using the method outlined in "NACA Report 640". The results of this process are presented below for both engines. This initial analysis was performed for two-bladed propellers and resulted in a propeller with a diameter of 7.2, and a blade pitch of 15 degrees being chosen for the Rotax 914, and a propeller with a diameter of 6.6, and a blade pitch of 15 degrees being chosen for the Rotax 912.

$Altitude\ (ft)$	10,000	10,000	Sea Level	Sea Level
$V\ (ft/s)$	161.37	146.7	132.03	117.36
$P\ (ft\ lbs/sec)$	53104	53104	54210	54210
ρ $(slugs/ft^3)$	0.001756	0.001756	0.002377	0.002377
$n\ (rps)$	37.72	37.72	37.72	37.72
C_s	1.205	1.095	1.043	0.9273
V/nD "J"	0.58	0.54	0.53	0.47
$D\ (ft)$	7.375	7.201	6.603	6.619
$c\ (ft/s)$	1036.7	1036.7	1116.2	1116.2
$Tip\ Mach$	0.857	0.835	0.711	0.711

Table 4 Propeller Analysis for Rotax 914

$Altitude\ (ft)$	10,000	10,000	Sea Level	Sea Level
$V\ (ft/s)$	161.37	146.7	132.03	117.36
$P\ (ft\ lbs/sec)$	42,900	42,900	42,900	42,900
ρ $(slugs/ft^3)$	0.001756	0.001756	0.002377	0.002377
$n\ (rps)$	40.38	40.38	40.38	40.38
C_s	1.224	1.113	1.064	0.946
V/nD "J"	0.59	0.55	0.5	0.47
$D\ (ft)$	6.773	6.605	6.539	6.183
$c\ (ft/s)$	1036.7	1036.7	1116.2	1116.2
$Tip\ Mach$	0.843	0.821	0.752	0.711

Table 5 Initial propeller analysis for Rotax 912

The results above and the resulting propeller efficiency curves were used during the optimization process. The propeller diameters of 6.6 and 7.2 seemed reasonable for our initial aircraft, which was around 25 feet in length, however, as our aircraft was optimized and became progressively smaller, ultimately being 10.4 feet in length, these propeller diameters became completely impossible. To remedy this, another propeller analysis was done to select a propeller with a feasible diameter. The results of this are seen below. Ultimately a 4-bladed prop with a blade pitch of 20 degrees and a diameter of 4.5 feet was selected.

$Altitude\ (ft)$	10,000	10,000	Sea Level	Sea Level
$V\ (ft/s)$	161.37	146.7	132.03	117.36
$P\ (ft\ lbs/sec)$	42,900	42,900	42,900	42,900
$\rho\ (slugs/ft^3)$	0.001756	0.001756	0.002377	0.002377
$n\ (rps)$	40.38	40.38	40.38	40.38
C_s	1.223	1.112	1.063	0.945
V/nD "J"	0.72	0.69	0.63	0.62
$D\ (ft)$	5.55	5.26	5.18	4.68
$c\ (ft/s)$	1036.7	1036.7	1116.2	1116.2
$Tip\ Mach$	0.696	0.659	0.601	0.543

Table 6 Final propeller analysis for Rotax 912

To see the resulting power available curves, see Figure 7 in Section III.2. What can be immediately noticed from this plot is the massive excess of power across the aircraft's flight envelope. In addition to the fact that this design significantly outperforms the design goals for every requirement except endurance, the most obvious way to improve this aircraft is to find a less powerful, lighter engine.

5. Stability

Static longitudinal stability is heavily dependent on the location of the center of gravity and neutral point. The final SNS design has a static margin of 22% based on the mean chord, indicating good longitudinal stability. See below a diagram of these locations on the aircraft. Additionally, 3 degrees of dihedral was included on the SNS design in the interest of providing sufficient lateral stability to serve as a stable camera platform.

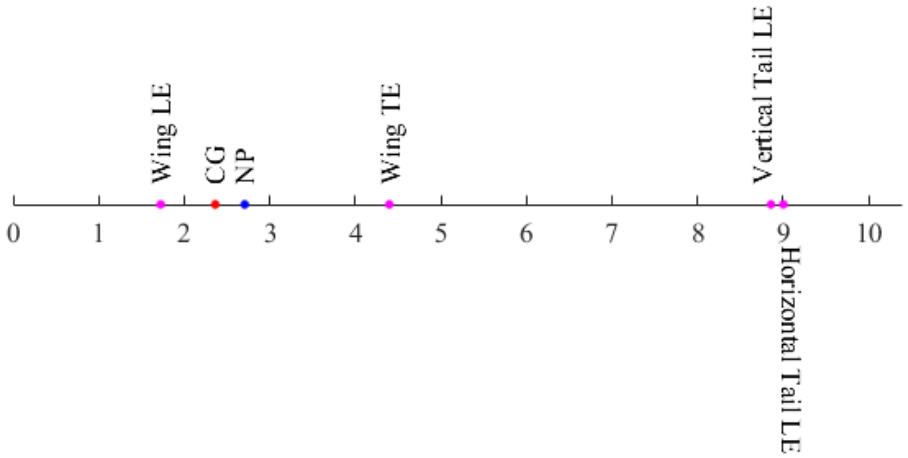

Fig. 6 Key locations along the longitudinal axis

6. Stability Derivatives

The stability derivatives for the SNS UAV are summarized below in Table 7. Many of these derivatives were estimated using analytical expressions found in textbooks such as McCormick's "Aerodynamics, Aeronautics, and Flight Mechanics" and Pamadi's "Performance, Stability, Dynamics, and Control of Airplanes".

Lift Derivatives	Values	Drag Derivatives	Values	Pitch Derivatives	Values
$C_{L,0}$	-0.0266	$C_{D,0}$	0.0223	$C_{m,0}$	0.0694
$C_{L,\alpha}$	5.8602	$C_{D,\alpha}$	0.2982	$C_{m,\alpha}$	-1.2912
$C_{L,\alpha dot}$	0.8869	$C_{D,\delta e}$	0.0180	$C_{m,\alpha dot}$	-3.9855
$C_{L,q}$	4.9266			$C_{m,q}$	-22.1384
$C_{L,\delta e}$	0.4010			$C_{m,\delta e}$	-1.7600
Side Force Derivatives	**Values**	**Roll Derivatives**	**Values**	**Yaw Derivatives**	**Values**
$C_{Y,\beta}$	1.2259	$C_{l,\beta}$	-2.58E-05	$C_{n,\beta}$	1.5317
$C_{Y,\delta r}$	0.2045	$C_{l,p}$	-0.5763	$C_{n,p}$	-0.132
		$C_{l,r}$	-0.0057	$C_{n,r}$	-0.0412
		$C_{l,\delta a}$	-0.1610	$C_{n,\delta a}$	0.0200
		$C_{l,\delta r}$	-0.00229	$C_{n,\delta r}$	-0.0917

Table 7 Stability derivatives for the SNS

Usually, many of these stability derivatives are found through experimental tests. For this reason, values for $C_{L,\delta e}$, $C_{D,\delta e}$, $C_{l,\delta a}$, $C_{l,\delta r}$, $C_{m,\delta e}$, $C_{n,\delta a}$, and $C_{n,\delta r}$ were difficult to find analytical estimates for. Therefore, for these derivatives, the values used in Simulink were kept the same as those of the RQ-2 Pioneer UAV. This is justified because the Pioneer UAV exhibits similar specifications to those of the SNS. For this same reason, the analytically estimated stability derivatives were also cross-checked with the RQ-2 Pioneer's values and all calculations fell within an order of magnitude difference. Some derivatives vary more than others, but this is expected because the SNS UAV is much more stable than the Pioneer, with a static margin of over 20%.

III. Performance

1. Requirements vs. Actual Performance

The primary design process for the Silent Night Surveillant was centered around meeting the critical design requirements. All values and figures in this section were computed under trim conditions at a cruise altitude of 10,000 ft unless otherwise stated. The requirements are compared with the true design parameters in Table 8 below.

Requirement	Target	Design	Margin
Endurance	24 hours	24.517 hours	2.15%
Stall Speed	90 fps	87 fps	3.33%
Top Speed	161.3 fps	214 fps	32.67%
Climb Angle	23 degrees	40.16 degrees	74.61%
Service Ceiling	10,000 ft	55,000 ft	450%

Table 8 Requirement targets vs design parameters

While all requirements were designed to be met, the 24-hour endurance was the primary design factor that consequently led to an over-design in some areas. As discussed in Section IV, input parameters to the SNS were varied until a final configuration was settled on, while ensuring the requirements in Table 8 were met. Values were selected so the final endurance of the SNS marginally met the required 24-hour window, resulting in only a 2.15% difference.

The large margins on top speed, climb angle, and service ceiling are because of a slightly overpowered engine for SNS UAV's needs, as discussed in Section II.3. While this was an unnecessary weight addition, the additional performance gain and service ceiling of 55,000 ft could prove to be useful for a high altitude surveillance UAV to meet Santa's yearly demands. Section III.5 will discuss a higher fidelity altitude analysis.

2. Power and Thrust Curves

Under steady-unaccelerated and trimmed flight aerodynamic forces are equal to their opposition. Lift is equal to weight and thrust is equal to drag. For a propeller-driven aircraft such as the SNS, it is useful to examine the power as a function of thrust times velocity. Figure 7 shows the Power Required in blue to maintain steady level flight and the Power Available in red from the chosen propulsion system in Section II.3.

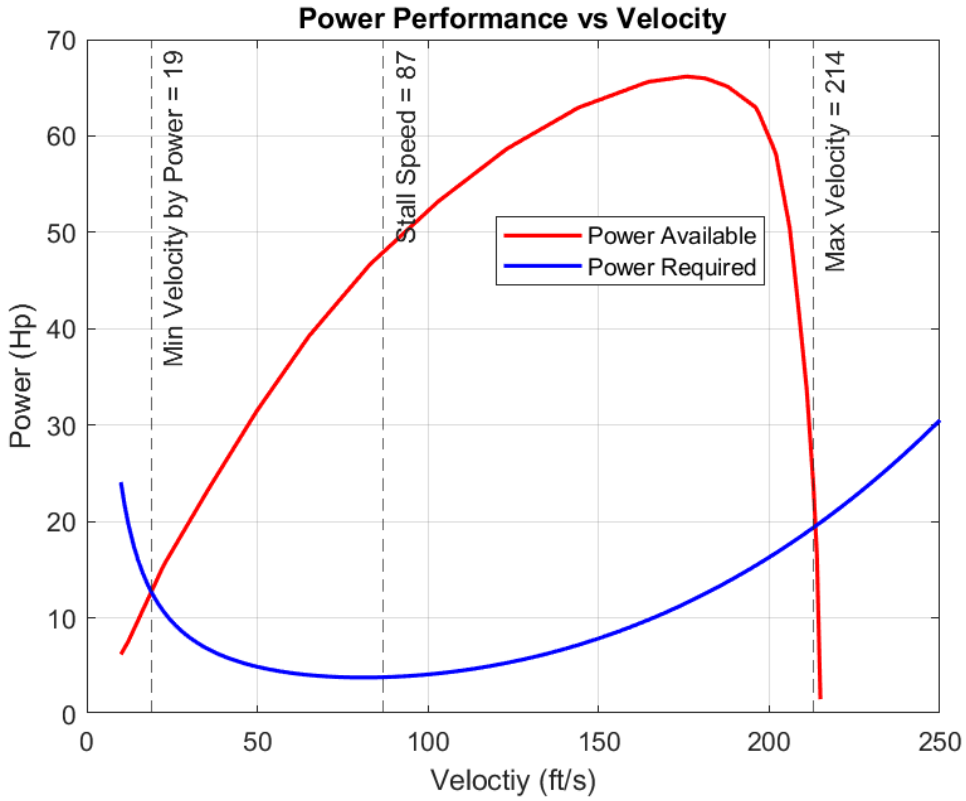

Fig. 7 Power performance of the SNS

Also noted in Figure 7 are the minimum and maximum velocities and the stall speed. Note that the minimum velocity of 19 fps from the powerplant is not physically achievable in flight since it falls well short of the stall speed of 87 fps. It is also worth looking at the thrust required and thrust available curves shown below in Figure 8.

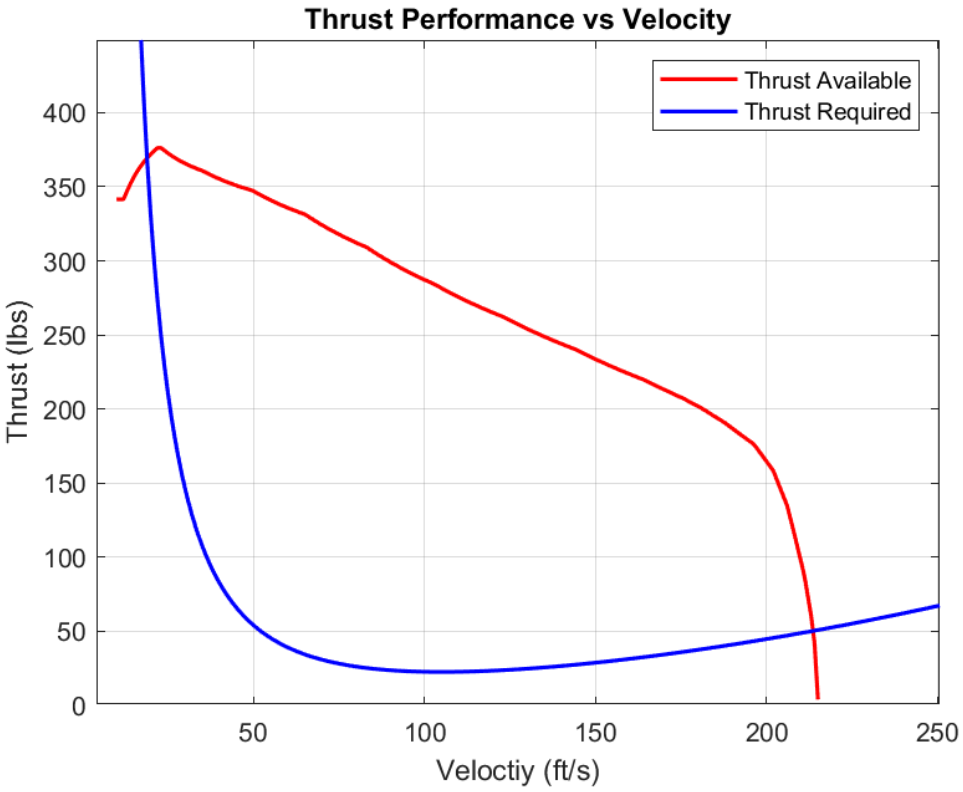

Fig. 8 Thrust performance of the SNS

3. Lift and Drag

A key aspect of designing the SNS was minimizing the drag on the aircraft. The total drag can be broken down into the following four categories: Induced, Parasitic, Trim, and Payload. Induced drag is dominantly created from the wing and tail downwash required to generate lift. Parasitic drag is due to the viscous skin friction effects from the frontal areas of the aircraft body. Parasitic drag was approximated using the component build-up method as described by Raymer. Trim drag comes from the elevator deflection required to keep the aircraft at steady level flight, and was estimated using the following equation from Pamadi. In this equation, the wing lift is calculated by subtracting the tail lift required for level flight from the total lift needed to maintain altitude. Essentially, this equation attributes trim drag to the additional lift needed by the tail to achieve 0 pitching moment.

$$\Delta C_D = k(C_{L,W}{}^2 - C_L{}^2)$$

The Payload drag is another parasitic drag term due to the camera protruding off the belly of the aircraft. The following figure details these different drag forces on the SNS over a range of velocities.

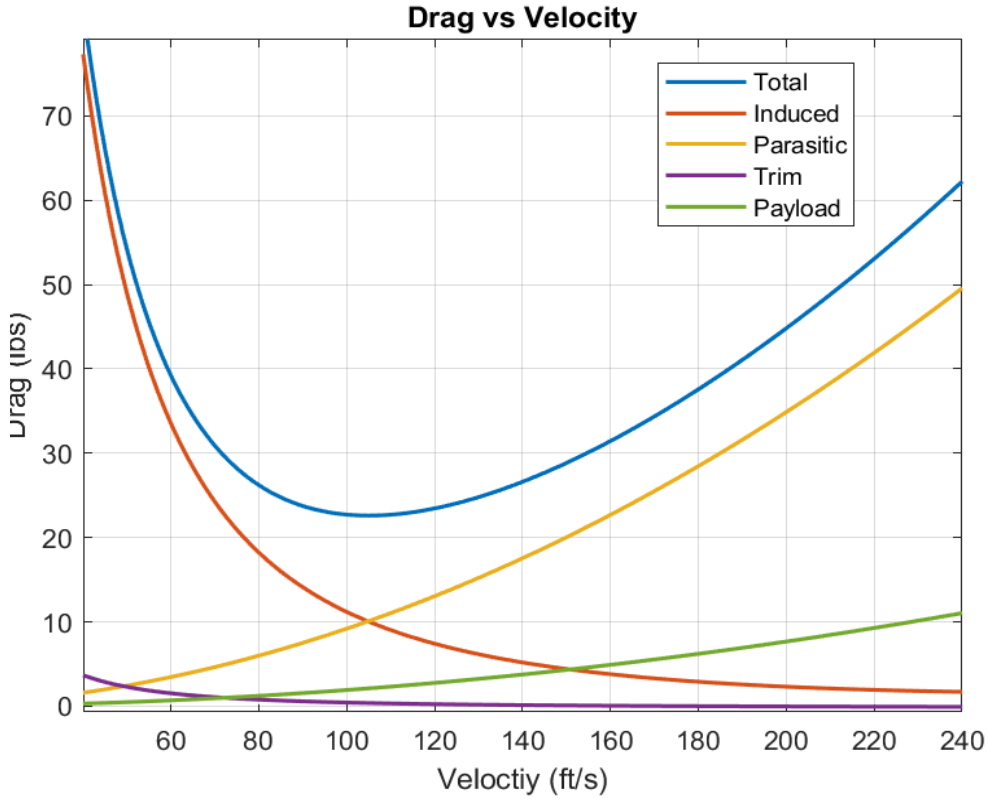

Fig. 9 Drag forces on the SNS

As shown in Figure 9, induced drag dominates at lower speeds while parasitic drag takes over at higher speeds. The trim drag in purple appears to be small if not negligible in the flight envelope of the SNS. This is likely due to having a relatively small horizontal stabilizer and an even smaller elevator. Even with elevator deflection the drag component remains small. It is also likely the parasitic drag component of the elevator deflection is underestimated in this analysis. The payload drag takes a similar form as the total parasitic drag as it is modeled as a protruding hemisphere.

An equally important design parameter is the lift generated by the aircraft. Since analysis was done for steady flight under trim conditions, it is given that the total lift force equals the total aircraft weight of 424.9 lbs. Therefore it is more useful to look at lift over drag ratios as shown in Figures 10 and 11.

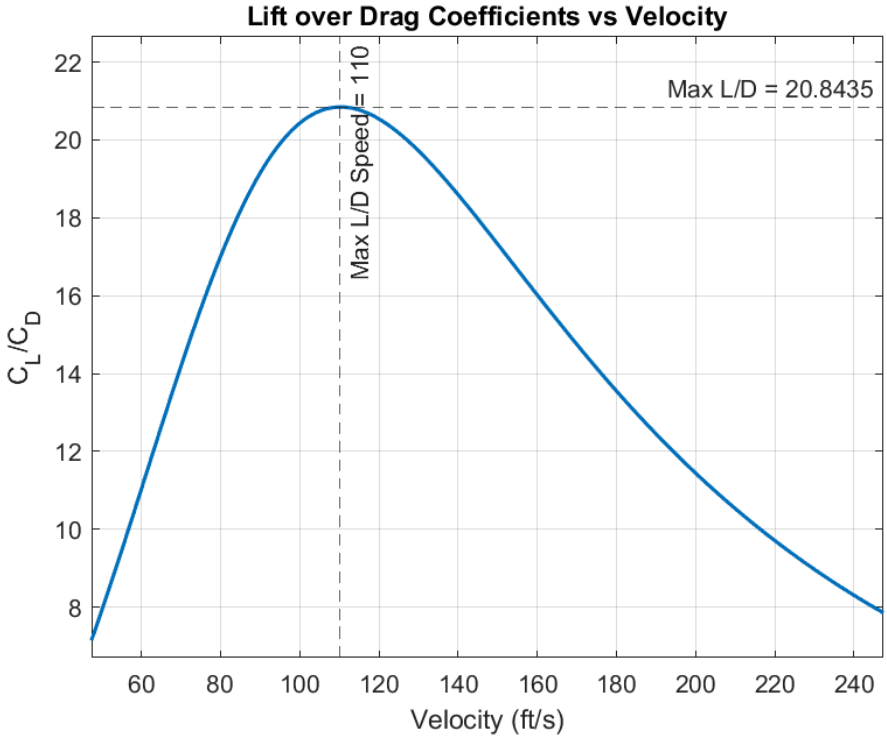

Fig. 10 Lift over drag ratio of the SNS

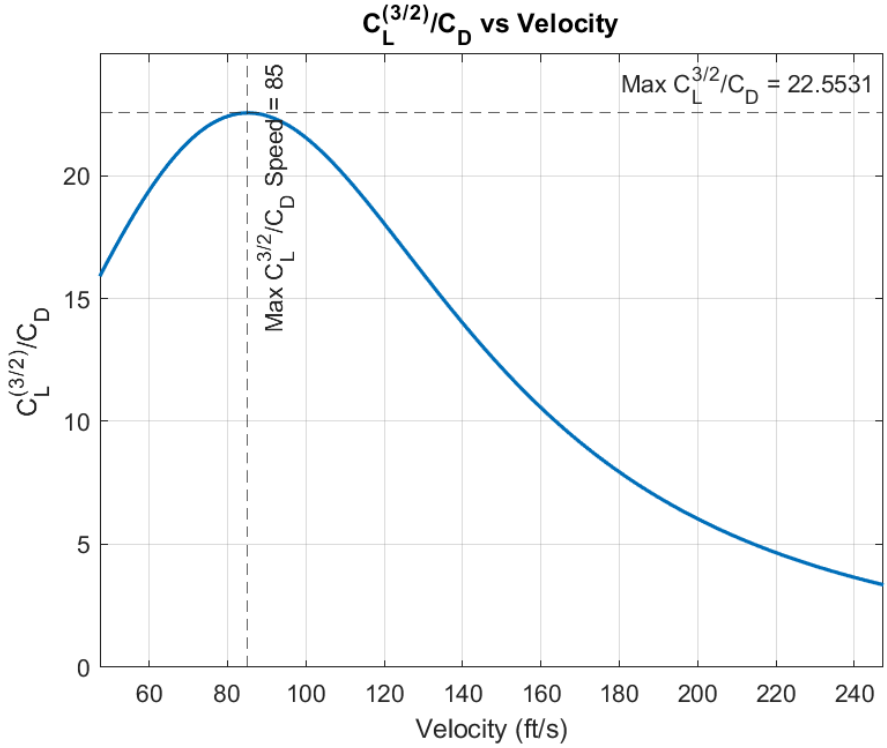

Fig. 11 $(\text{Lift})^{3/2}$ over drag ratio of the SNS

4. Trim Details

This section will examine additional trim analysis and performance characteristics of the SNS. As previously mentioned, the elevator must deflect to maintain trim conditions for different cruise speeds or attitudes. This relation is shown below.

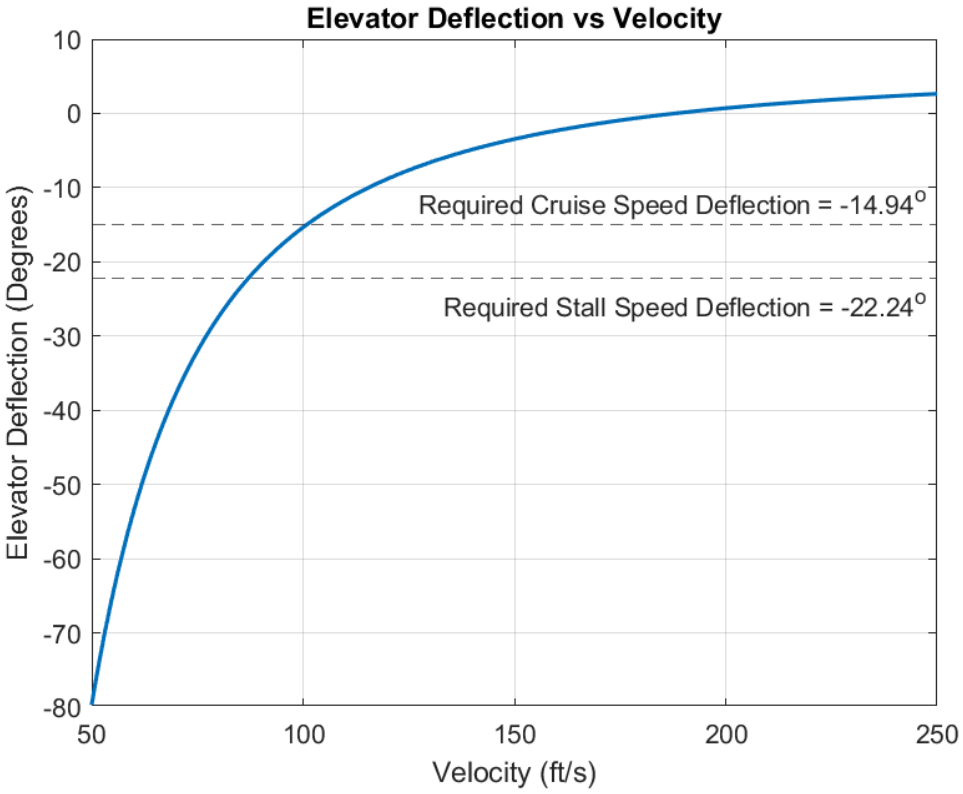

Fig. 12 Elevator deflection to maintain trim conditions

Note that in Figure 12 a negative elevator deflection refers to an upwards movement in the elevator to create a pitch-up moment necessary for cruise conditions at lower speeds. It should also be noted that the labeled -22.24° deflection for the SNS stall speed may be physically impractical due to cable pulley or actuator limits. If that is the case, a design with a larger elevator surface would be needed to change trim conditions without excessive deflections.

The following figure details the aircraft's endurance over the velocity range. This is of particular importance because the 24-hour endurance requirement is only satisfied for a select range of velocities and is only maximized at one velocity.

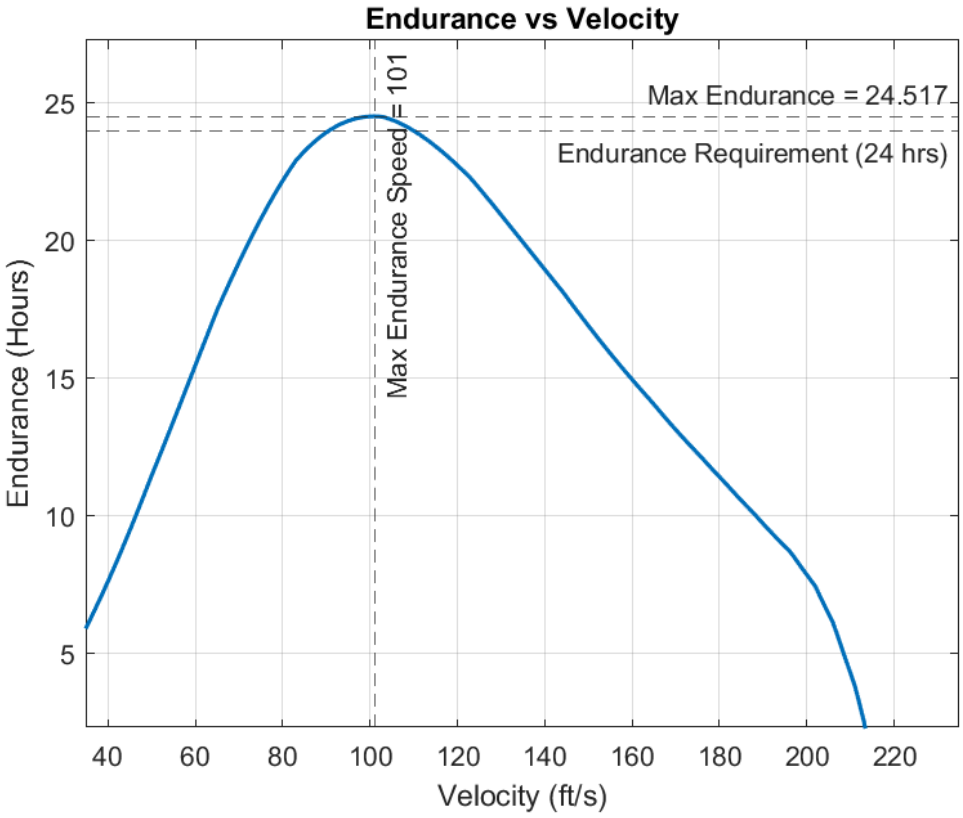

Fig. 13 Endurance performance of the SNS

From Figure 13, there is an approximately 20 fps window where the SNS can fly and be able to meet the 24-hour airborne requirement. At a velocity of 101 fps, maximum endurance is achieved, providing a half-hour margin on the requirement. This is correspondingly our selected cruise velocity for the Simulink input. The remainder of the performance parameters for the SNS at a cruise altitude of 10,000 ft are displayed in the figures below

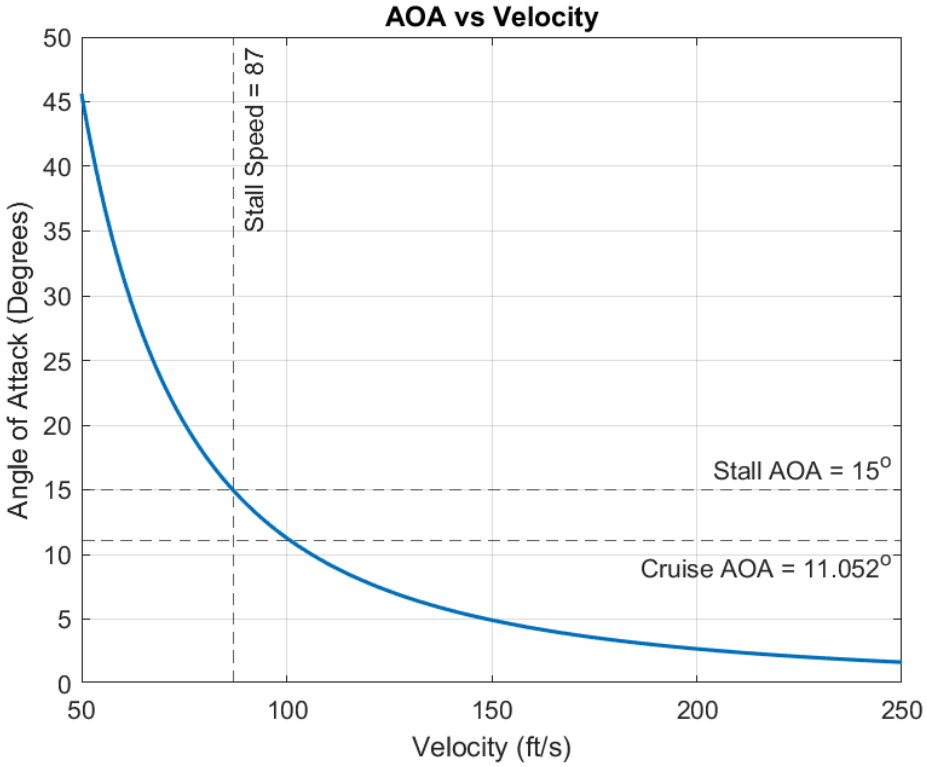

Fig. 14 Angle of attack performance of the SNS

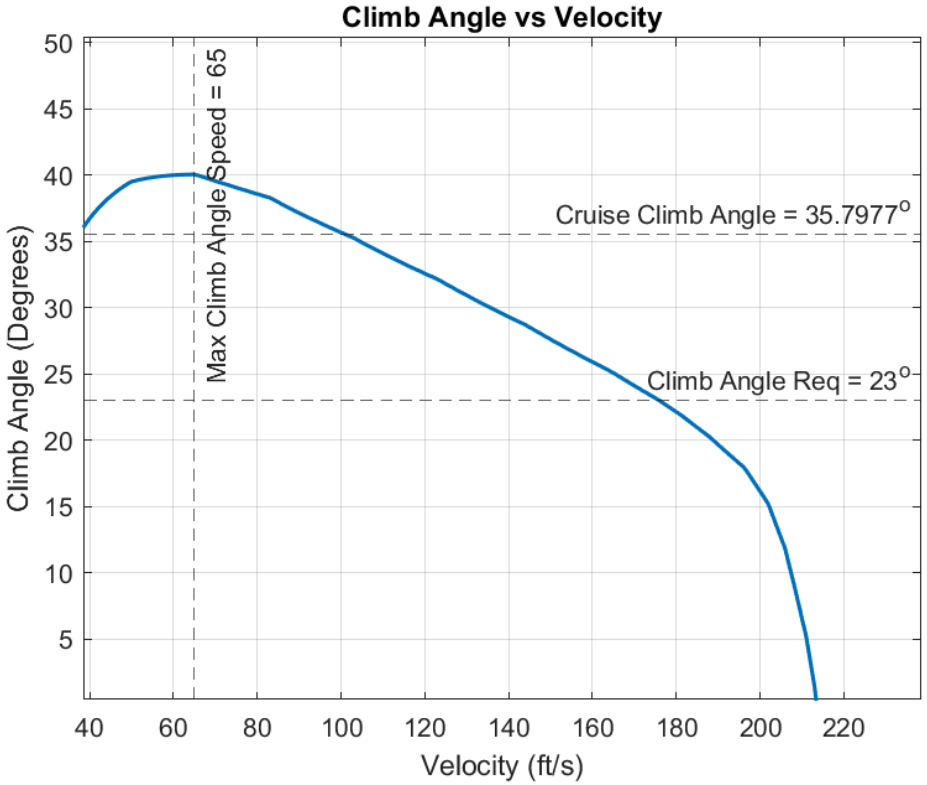

Fig. 15 Climb angle performance of the SNS

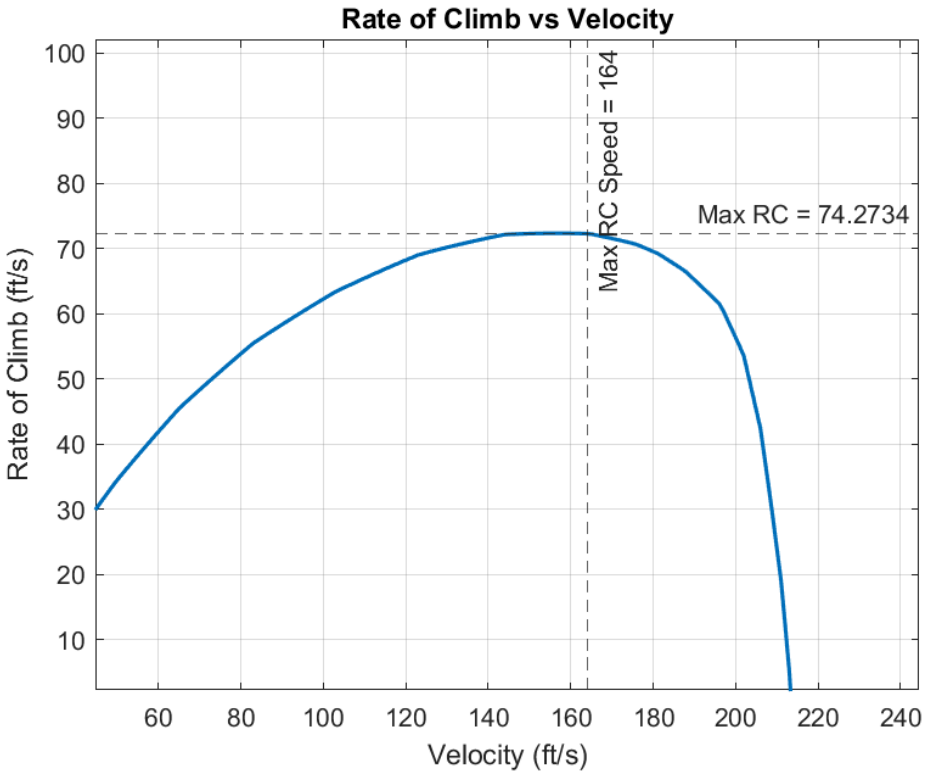

Fig. 16 Rate of climb performance of the SNS

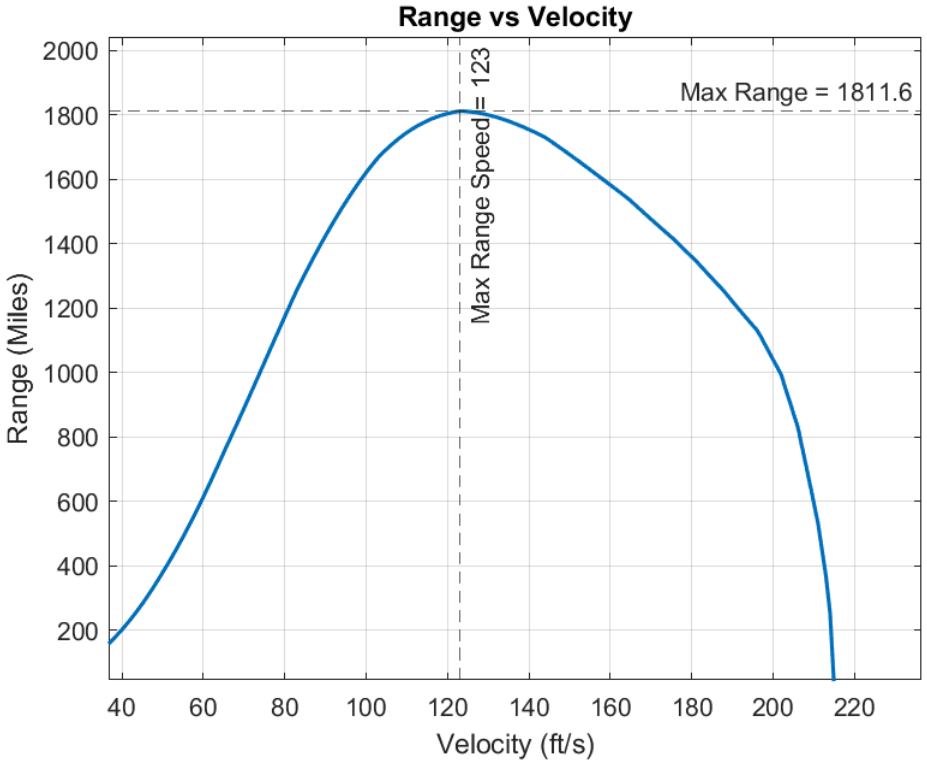

Fig. 17 Range performance of the SNS

The above figures show the angle of attack, climb angle, rate of climb, and range performance parameters respectively. Maximum and cruise values are denoted along with corresponding velocities. Figure 16 also shows the climb angle requirement in Table 1 being satisfied.

5. Altitude Analysis

To test the performance parameters of the SNS across a range of altitudes a higher fidelity analysis was performed. As a surveillance UAV, we deem it appropriate for the SNS to 5be capable of high-altitude flight. For a UCLA student of particular naughtiness, it may be necessary to alter mission requirements and surveil from a higher cruise altitude to ensure the secrecy of Santa's operation.

To perform this analysis, the performance of the SNS was tested for the following altitudes: Sea Level (0 ft), Cruise (10,000 ft), 32800 ft, 50840 ft, and 55,7600 ft. The following figure shows the power required for the SNS to fly level flight at these altitudes.

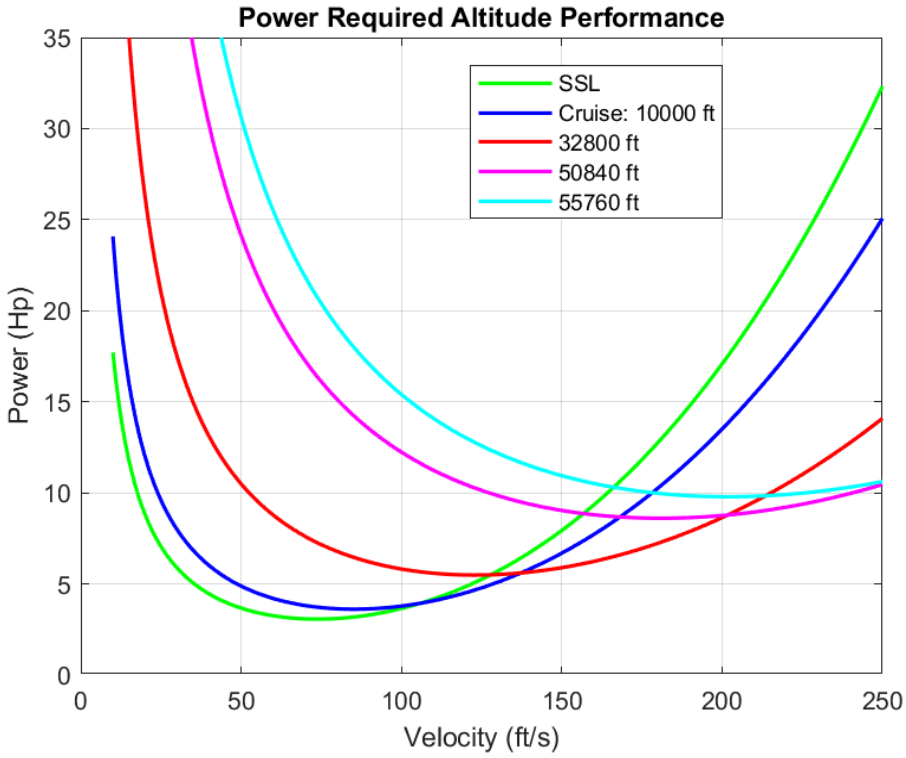

Fig. 18 Power required altitude performance of the SNS

Notice in Figure 18 that as altitude increases the power required of the aircraft shifts diagonally to the right of the graph. This is because density decreases dramatically as altitude increases, forcing the SNS to fly faster to maintain cruise conditions of lift equals weight. A faster cruise speed therefore increases the total parasitic drag on the aircraft, resulting in the upward shift of power required. Similarly, the power available of the SNS can be examined as altitude increases, as shown in the figure below.

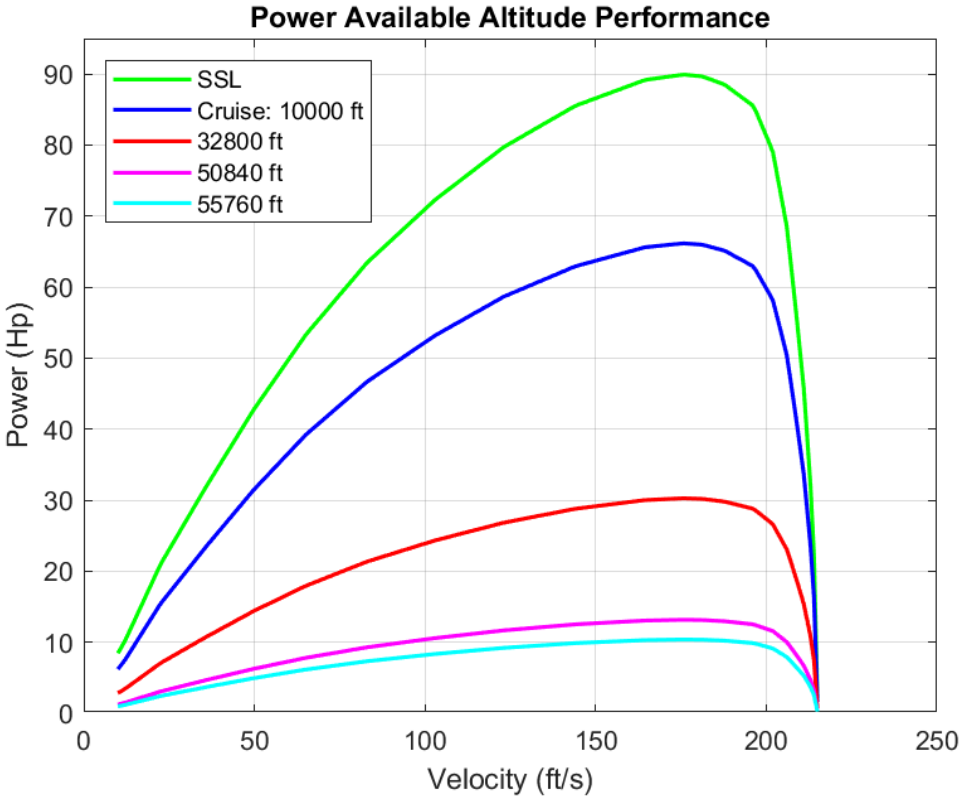

Fig. 19 Power available altitude performance of the SNS

Due to the decreasing density of the air, the equipped engine and propeller can produce much less power as the altitude increases. Thin air means less oxygen to combust in the reciprocating piston engine and less mass to be pushed from the propeller, resulting in the power drop seen in Figure 19. Flying at Standard Sea Level would yield the best performance, however, that is not practical for an aircraft and the mission requirements of the SNS.

The difference between power available and power required, or excess power, represents the margin of the aircraft's performance. At the point where the two curves are tangent but do not overlap the aircraft can be said to be at its absolute ceiling. This is approximately shown below for the case of a 55,760 ft cruise altitude.

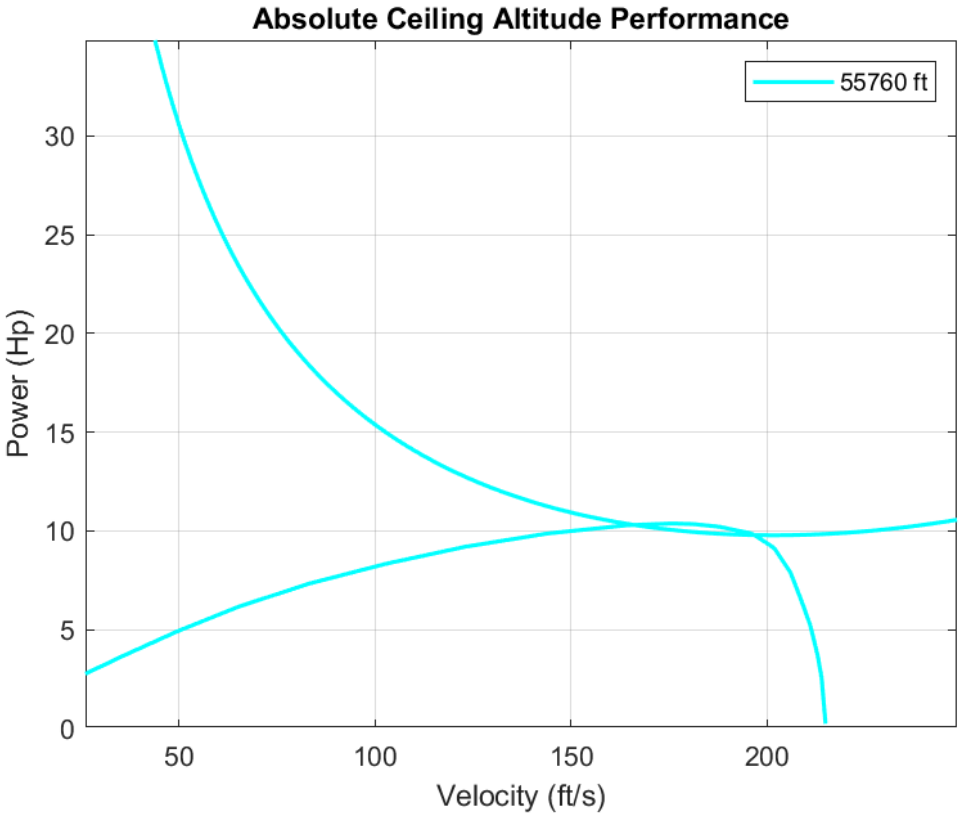

Fig. 20 Absolute ceiling altitude performance of the SNS

There is still a very slight overlap of the two curves shown in Figure 20 around the 180 fps region, so the true absolute ceiling can be estimated as 56,000 ft. This is the altitude where the aircraft achieves a climb rate of 0 and cannot actually be achieved in flight. The service ceiling, where the SNS achieves a climb rate of 100 fpm, can also be estimated in the following figure.

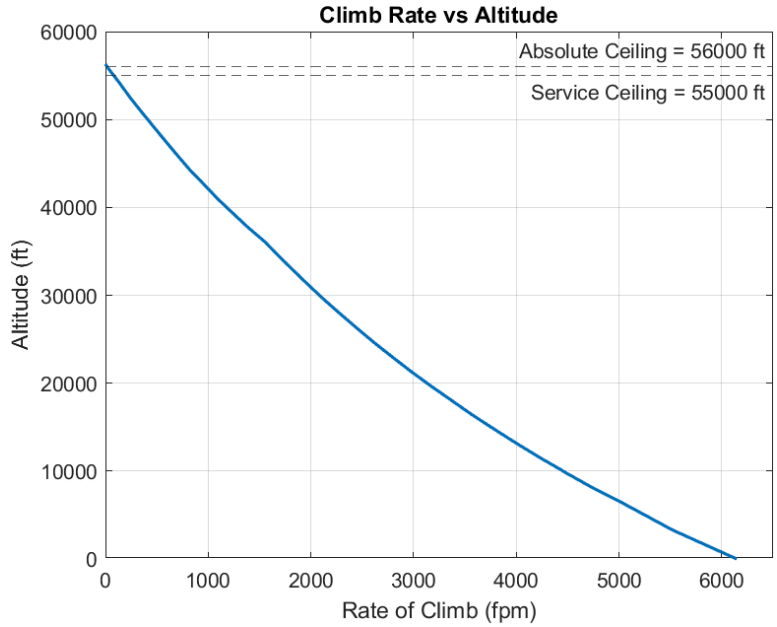

Fig. 21 Rate of climb vs altitude for the SNS

At 100 fpm, the SNS has a service ceiling of approximately 55,000 ft. The curve in Figure 21 exponentially decays, highlighting the benefits of a high climb rate to lower cruise altitudes. In the context of the SNS's mission, the endurance can be calculated and compared for the range of altitudes. This is shown in the figure below.

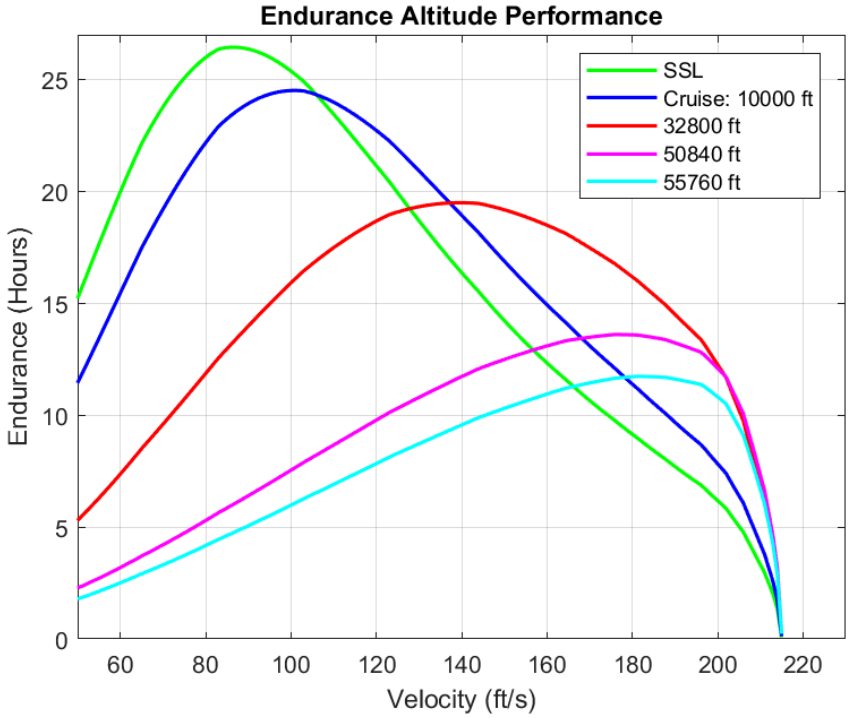

Fig. 22 Endurance altitude performance of the SNS

As mentioned in Section IV.4, the SNS was designed at a cruise altitude of 10,000 ft to just marginally meet the 24-hour endurance requirement. Therefore, at higher altitudes the endurance drops and will not meet the requirement. However, it is useful to examine altered missions where high-altitude surveillance outweighs the length of surveillance. For example, at 50,840 ft the SNS can survey for approximately 13.5 hours flying at a speed of roughly 180 fps.

IV. Optimization

1. Strategy

Before the SNS can be optimized, an initial aircraft needs to be obtained. A requirements-driven approach is taken to design an initial working aircraft that satisfies all the mission requirements. In this development phase, theoretical flight dynamic equations such as those provided in the MAE 154S slide decks, are implemented in code to produce initial aircraft specifications. These unoptimized specifications are considered quantities of interest and serve as initial values for the optimization inputs-driven approach described in the following paragraph.

The goal of this work is to design the lightest aircraft that satisfies the mission requirements. For this reason, an inputs-driven optimization approach is implemented using a Monte-Carlo-style method. 1,000 data points are randomly sampled around each quantity of interest. In total, this consists of thirteen quantities of interest being randomly sampled. These quantities are shown in Table 9 below.

Wing Area (*ft²*)	S_W	**Fuselage Length (*ft*)**	l
Horiz. Tail Area (*ft²*)	S_{HT}	**Fuel Weight (*lbs*)**	W_f
Vert. Tail Area (*ft²*)	S_{VT}	**Taper Ratio**	TR
Elevator Area (*ft²*)	S_E	**Tail Incidence Angle (°)**	i_t
Wing Aspect Ratio	AR_W	**Wing Location**	x_W
Horiz. Tail Aspect Ratio	AR_{HT}	**Payload Location**	x_{Pl}
Vert. Tail Aspect Ratio	AR_{VT}		

Table 9 Quantities of interest for optimization

The resulting Monte Carlo randomized aircraft are then checked to see if they satisfy every mission requirement. In the code, the following checks are performed.

- ☐ Has an endurance of 24 hours.
- ☐ Has a maximum climb angle greater than 23°.
- ☐ Has a maximum rate of climb greater than propeller capabilities (100 fpm).
- ☐ Has a static margin greater than 0.
- ☐ Has a maximum AoA less than 15° to prevent stall.
- ☐ Has a maximum velocity greater than the minimum top speed (161.3 fps)

Each Monte Carlo aircraft and its randomized quantities of interest are then saved and compared. Fourteen different plots are produced with failing aircraft in red and passing aircraft in green: one plot showing the aircraft at each varied quantity of interest and one plot showing each aircraft with the overall weight. The top twenty-five lightest aircraft are also displayed as blue asterisks, with the lightest aircraft displayed as a solid yellow dot. These plots are seen in Figures 24 and 25 shown in the following results section.

This is an iterative process and these plots are produced to make it easy to recognize general trends in passing aircraft. These general trends are then used to inform the trajectory of convergence on an optimal aircraft design. For example, if all the top twenty-five passing aircraft have higher wing aspect ratios, the next Monte Carlo iteration will randomly sample at higher wing aspect ratios. Convergence is achieved when there is little to no change in aircraft specifications between successive iterations. Figure 23 demonstrates the flow of this optimization approach. The following section displays the results of this process.

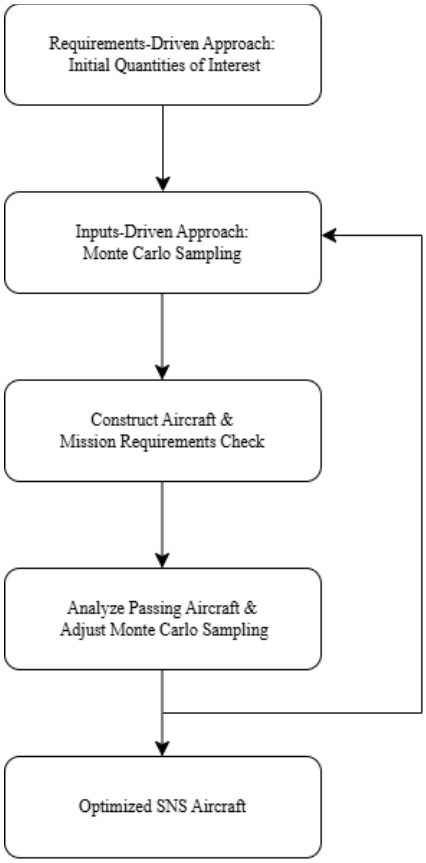

Fig. 23 Optimization strategy flow chart

2. Results

After performing the requirements-driven approach outlined above, initial aircraft specifications were found. These specifications are shown in Table 10 below.

Wing Area (*ft*^{2})	112	**Fuselage Length (*ft*)**	25
Horiz. Tail Area (*ft*^{2})	22	**Fuel Weight (*lbs*)**	57
Vert. Tail Area (*ft*^{2})	17	**Taper Ratio**	0.5
Elevator Area (*ft*^{2})	$S_{HT}/4$	**Tail Incidence Angle (°)**	2
Wing Aspect Ratio	20	**Wing Location**	*l*/2
Horiz. Tail Aspect Ratio	4	**Payload Location**	*l*/2
Vert. Tail Aspect Ratio	3		

Table 10 Initial quantities of interest from the requirements-driven approach

These values are then used to seed the inputs-driven optimization approach. As a reminder, this approach uses a Monte Carlo method to vary aircraft specifications and find the lightest, optimal aircraft. After the first iteration, the following plots in Figure 24 are produced.

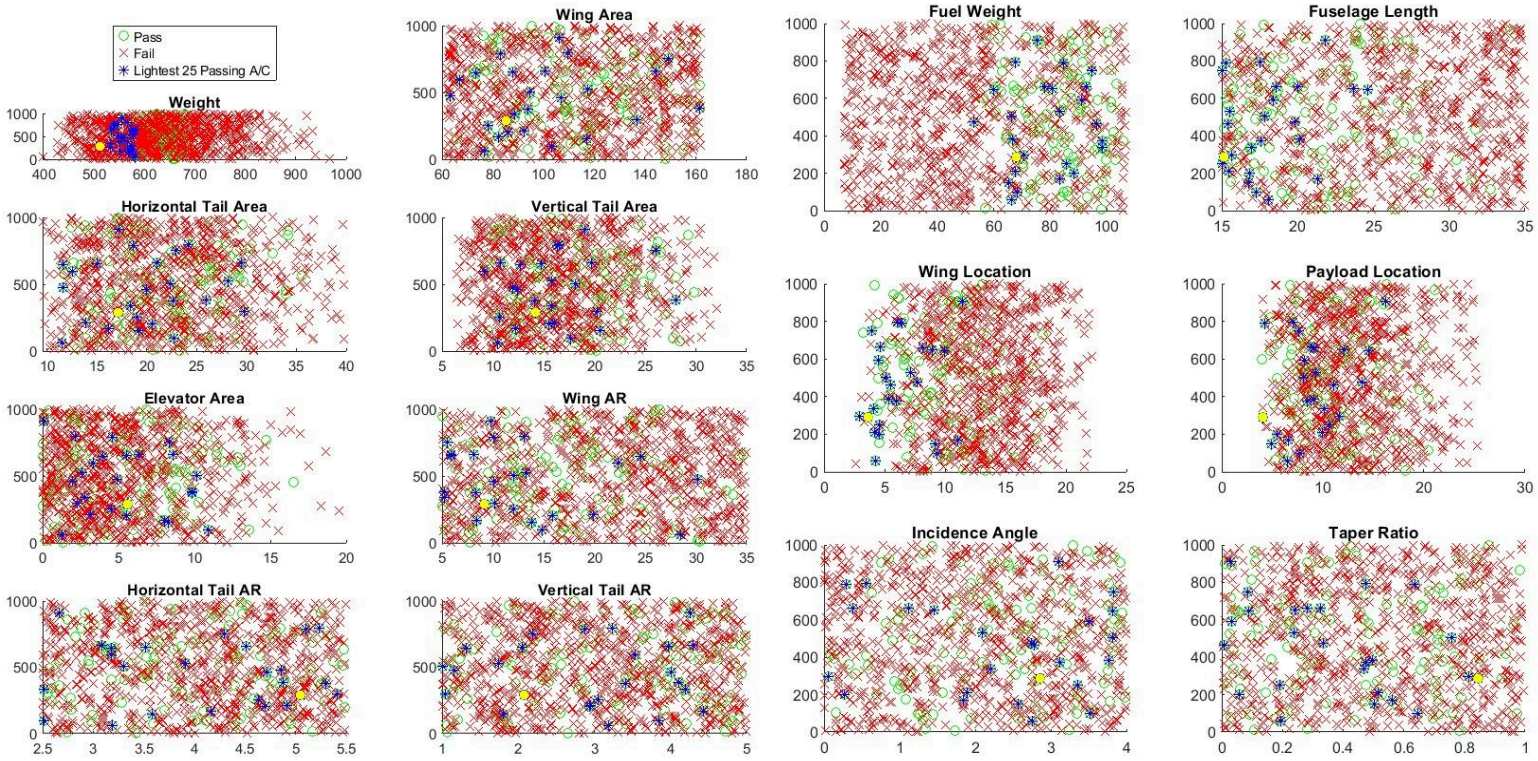

Fig. 24a & 24b Inputs-driven approach first iteration

From these results, there are a few interesting things to take note of. In general, passing aircraft exhibit lower horizontal tail areas, wing aspect ratios, and wing taper ratios. Additionally, passing aircraft have shorter fuselage lengths with wings pushed more towards the nose of the aircraft and higher fuel weights. These quantities of interest were then shifted in the following optimization iteration. In total, five to six iterations were performed with the final iteration results displayed in Figure 25 below.

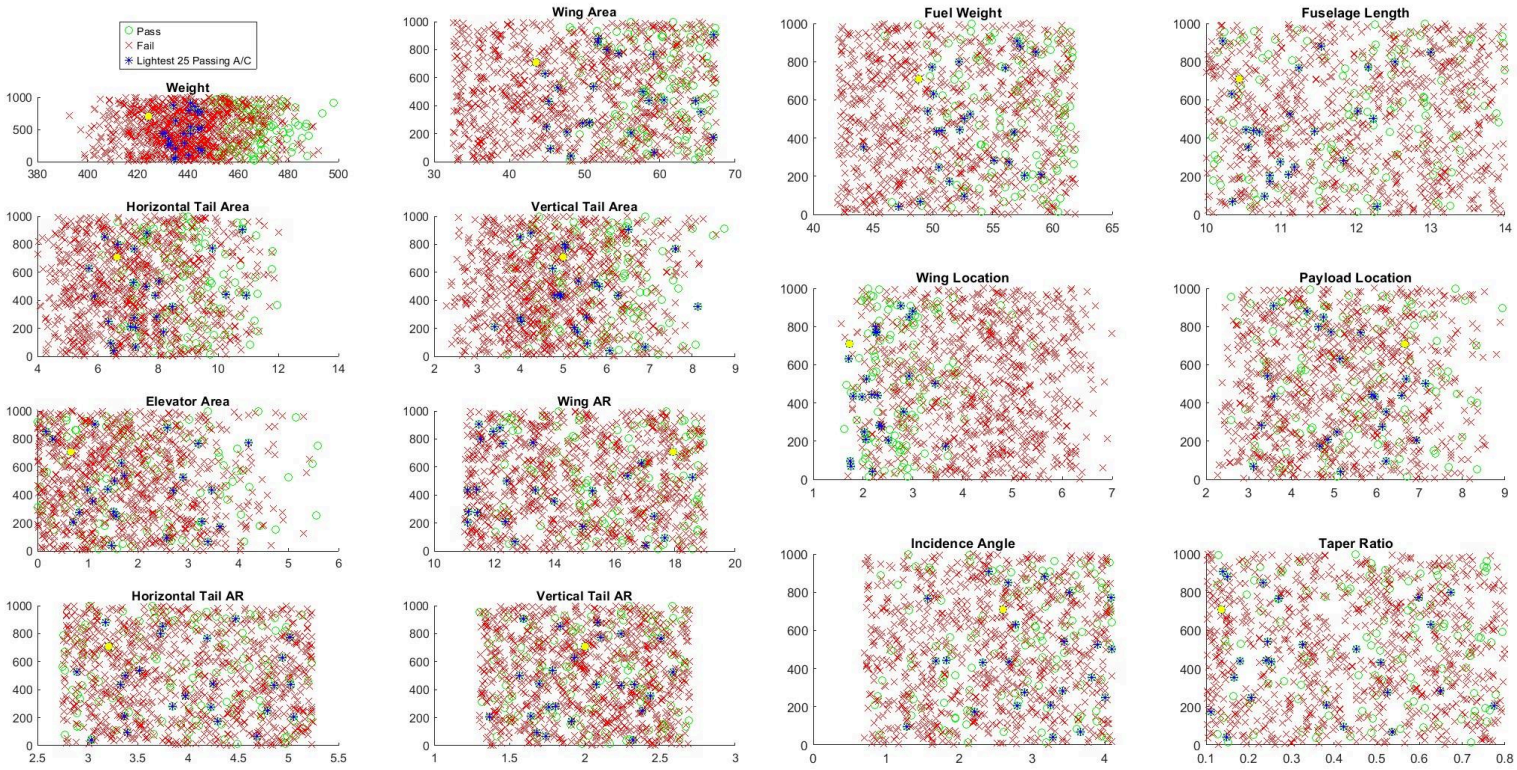

Fig. 25a & 25b Inputs-driven approach last iteration

In this last iteration, many of the quantities of interest have evenly spread themselves out across the parameter space. Additionally, total aircraft weight has significantly decreased, dropping to 424.9 lb from a starting weight of about 700 lb. This analysis was also performed for another, lighter aircraft engine. This analysis resulted in an even lighter aircraft that met all the mission requirements. Figure 26 demonstrates the weight evolution of each iteration process.

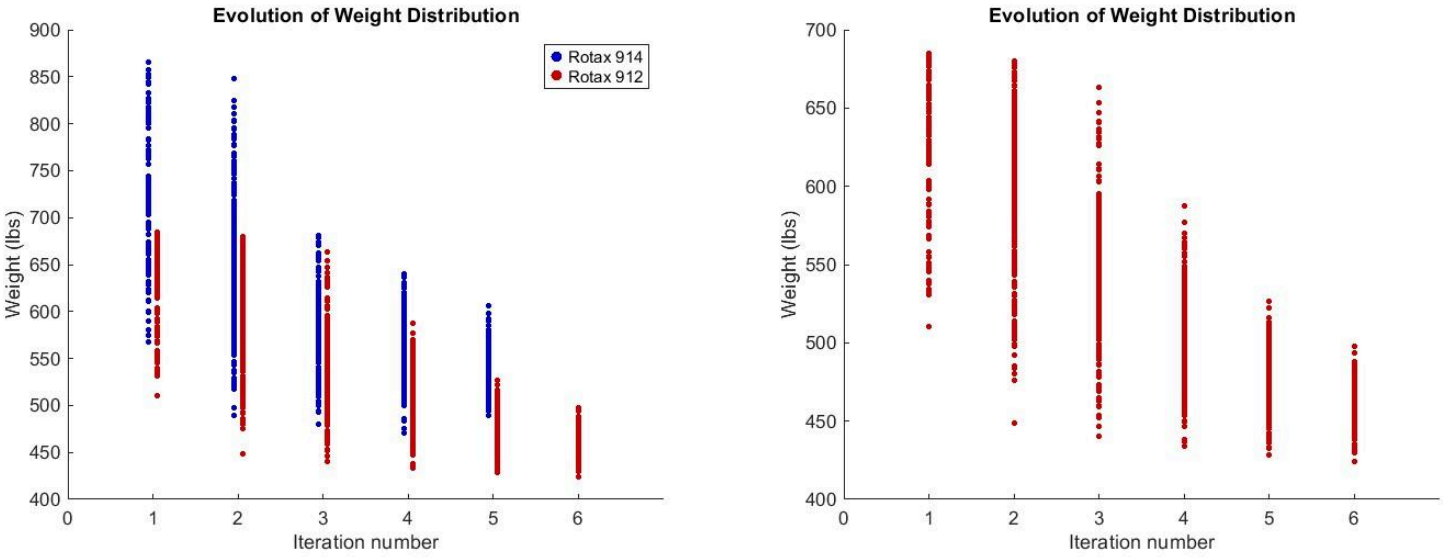

Figure 26a & 26b Weight evolution using two different aircraft engines

Note that, as mentioned in Section II, an even lighter engine could have been investigated. However, due to time constraints, the analysis concluded with the Rotax 912 engine. With that said, as observed in Figures 26a and 26b, a general trend towards lighter engines is evident.

V. Simulation and GNC

1. GNC Strategy

The GNC strategy chosen for this mission is Waypoint Navigation. This strategy was chosen because the aircraft is designed to circle the perimeter of the UCLA campus until it finds its target. Once the target is found, the aircraft is designed to set waypoints around the target and circle them until enough data is acquired and the mission is complete.

2. Modified Simulink

The provided Simulink code did not consider how air density changes as a function of altitude. In this mission, the SNS reaches high altitudes where air density cannot be considered constant. Therefore, to add fidelity to the Simulink code, the "Aircraft Dynamics" block was modified to account for air density changes. This is seen in Figures 27 and 28 below.

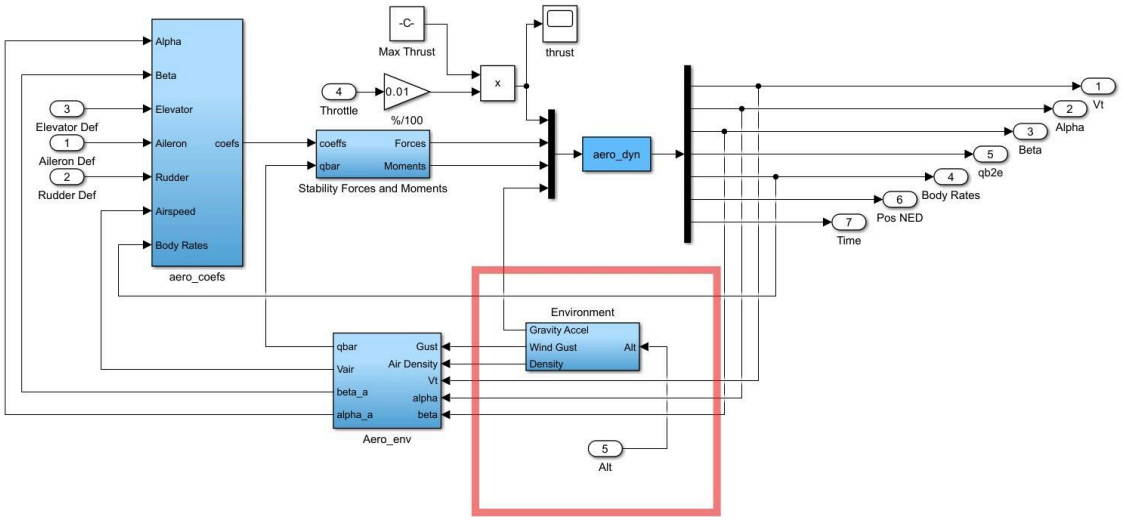

Figure 27 Inside the "Aircraft Dynamics" block, the "Environment" block was modified.

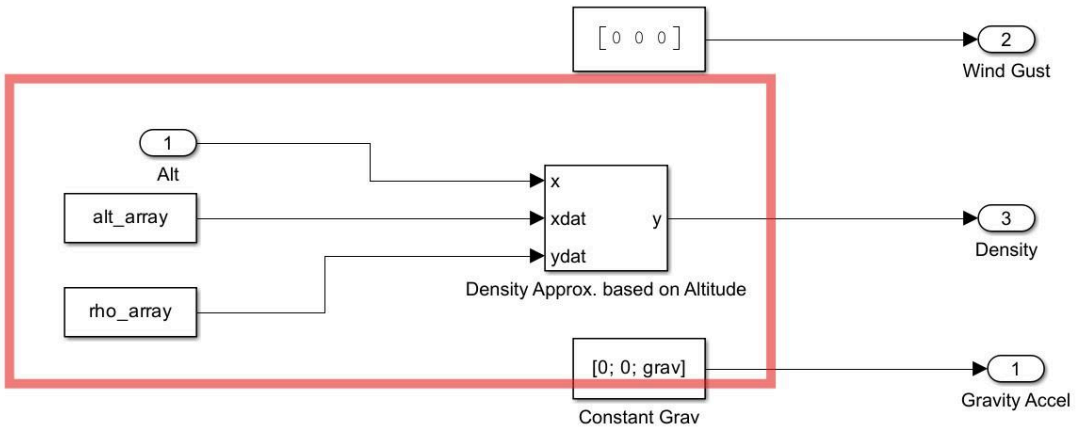

Figure 28 Inside the "Environment" block, air density was interpolated from a set of table look-up values

3. Simulink Output

After implementing the GNC strategy in Simulink and modifying the code to add fidelity to air density and altitude changes, the simulation is run. Two sets of figures are displayed below. Figures 29 and 30 demonstrate the SNS in search mode before the target is acquired. As previously mentioned, in this mode waypoints are set around the perimeter of the UCLA campus, and the aircraft traverses these waypoints until the target is found.

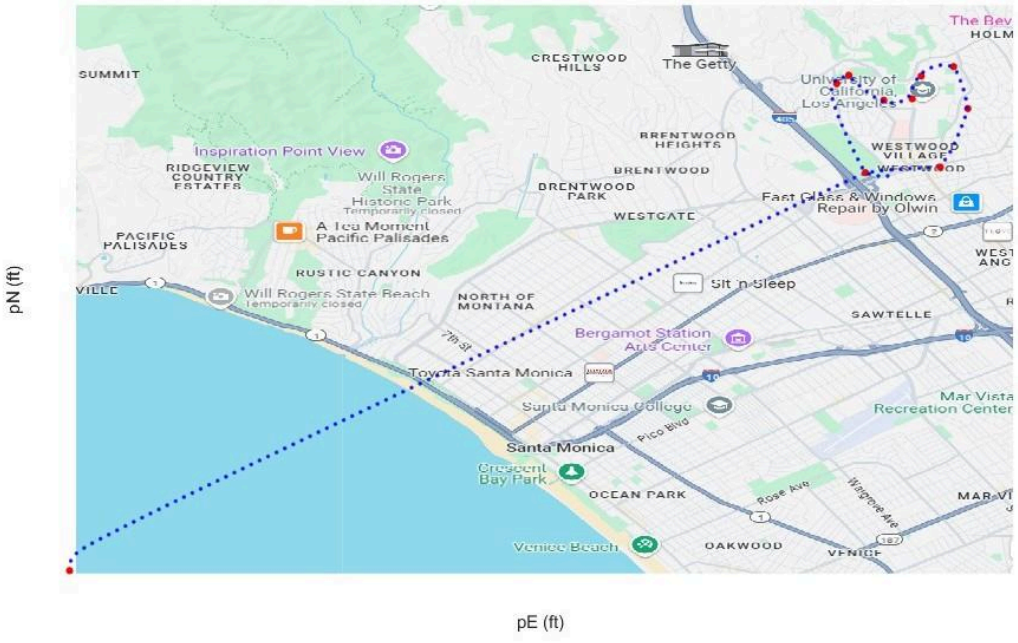

Figure 29 The SNS sets waypoints around the perimeter of the UCLA campus until the target is identified.

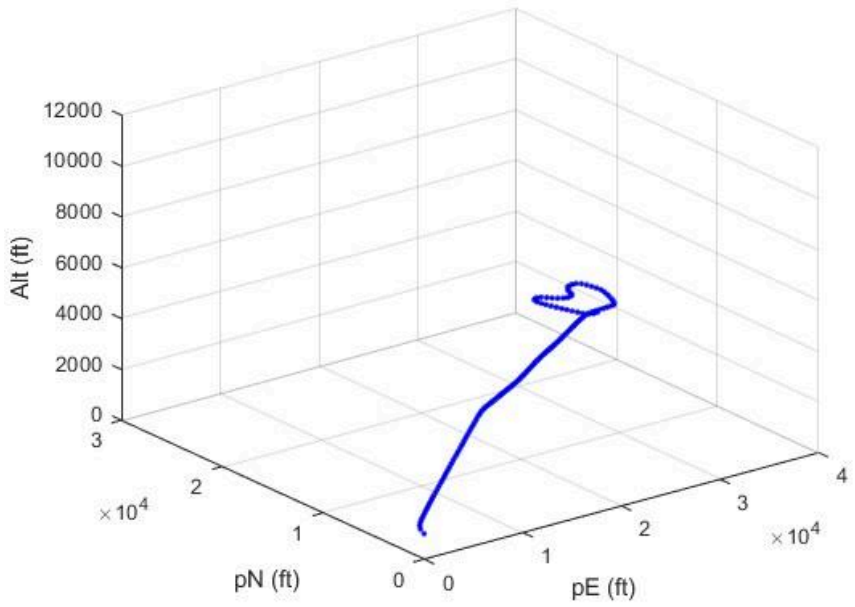

Figure 30 **The Silent Night Surveillant takes off from the offshore Christmas Carrier and circles UCLA at altitude.**

Figures 31 and 32 demonstrate the aircraft in data acquisition mode. In this mode, the aircraft circles the target by continuously setting waypoints around them. This is done until the mission is complete.

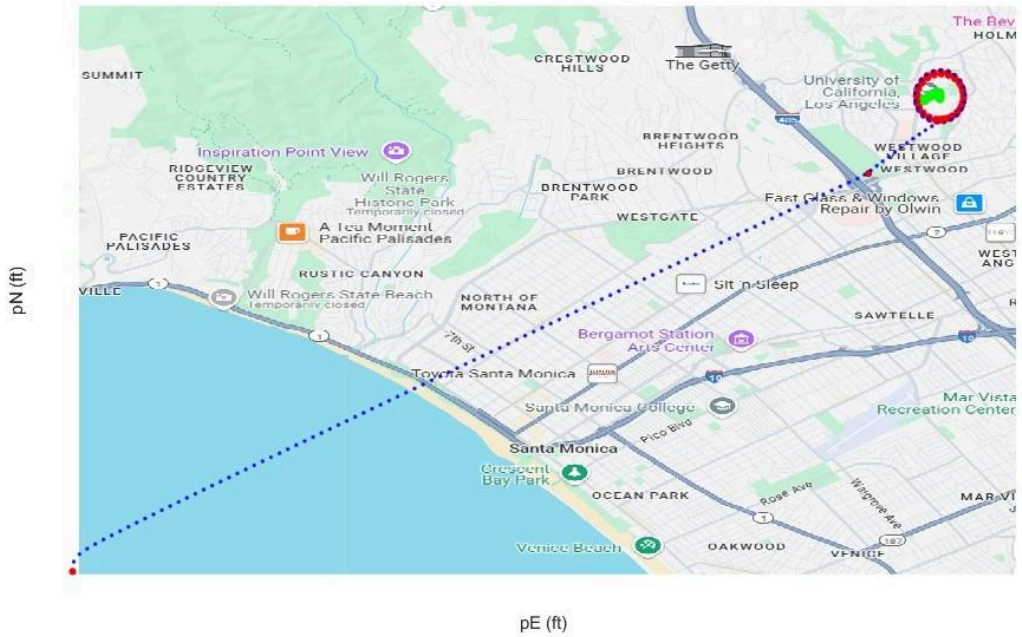

Figure 31 **The Silent Night Surveillant circles the target when the target is found.**

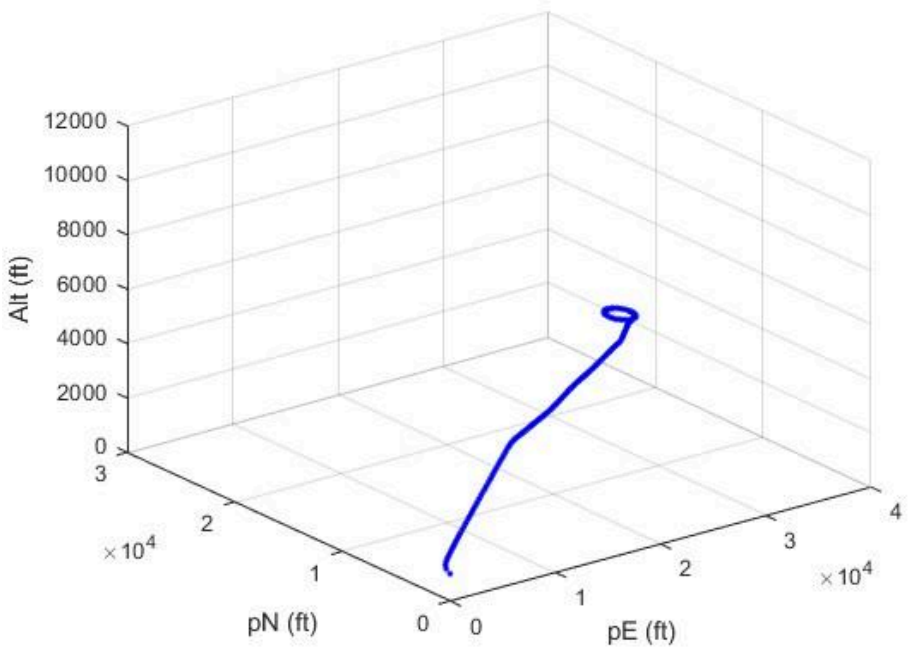

Figure 32 **The Silent Night Surveillant takes off from the offshore Christmas Carrier and circles the target at altitude.**

Note that in these figures, the SNS is only achieving an altitude of 3,000 ft. This is only to display the mission in simulation. In reality, and as discussed earlier in this report, the SNS operates at an altitude of 10,000 and launches adequately far away to achieve altitude before arriving at the UCLA campus.

VI. Conclusion

1. Summary

In summary, Santa recruited top engineers to design him the Silent Night Surveillant, tasked with conducting covert, naughty-nice assessments of the UCLA student body. The design process started with a requirements-driven approach, with the goal of obtaining an initial, mission-requirement-satisfying aircraft. The specifications of this aircraft were then used to seed an input-drive Monte Carlo optimization approach, which sampled 1,000 data points around each

quantity of interest. The resulting Monte Carlo aircraft were then passed or failed based on the mission requirements, and the passing aircraft were used to inform the trajectory of convergence on an optimal aircraft. Five to six iterations were performed for two different engines and an optimized, low-weight aircraft was found.

2. Caveats

As mentioned throughout the report, there are some caveats to the SNS UAV design. For one, airfoils were not fully investigated. With an optimized airfoil for the wing and horizontal tail, more lift could be achieved leading to smaller wings and a lower overall weight. Additionally, lighter engines could have been run through the optimization process to obtain an even lighter final aircraft. Due to time constraints, only two engines were investigated.

Additionally, payload drag was estimated using online hemisphere drag coefficients. This leads to inaccuracies in drag estimates and performance qualities. With a more accurate drag estimate, a less powerful, lighter engine could be used resulting in a lighter overall aircraft design.

The propeller specifications used during optimization are also a major caveat, as those propellers were unsuitable for the final size of our aircraft. Ideally, the optimization would've been done with the final propeller design, and with more time the optimization could have been redone to accomplish this. As a solution for the ultimate aircraft design, a smaller propeller was developed that still met the mission requirements, however, it was difficult to apply the NACA 640 report methods to undersized propellers, and therefore there may be some error in the resulting efficiency curves used in the power available calculations.

Regarding stability derivatives, it was also very difficult to find accurate analytical estimates. Many stability derivatives are typically found through experimental tests, so analytical estimates found in textbooks like McCormick's "Aerodynamics, Aeronautics, and Flight Mechanics" and Pamadi's "Performance, Stability, Dynamics, and Control of Airplanes" cannot fully be trusted. With that said, analytical estimates were unable to be found for a nontrivial number of the SNS UAV's stability derivatives. For those, the stability derivatives from the Pioneer UAV were used because the SNS UAV exhibited similar specifications.

3. Future Improvements

Given more time, the SNS UAV could have been further optimized in weight. One notable feature of the optimization process was the amount of time it took to analyze trends and adjust sampling ranges accordingly. With more time, a more streamlined and automated process would be worthwhile to implement to quickly obtain an optimized aircraft. Additionally, with more time, additional airfoils and aircraft engines could be explored which would allow increased performance and weight saving. Lastly, Simulink would also be fun to play with. Based on the location of the target, different altitude adjustments could be made to achieve a clearer view. Alignment with the aircraft carrier upon landing could also be implemented.

VII. Acknowledgments

[1] D. Toohey, MAE 154S, Mechanical and Aerospace Engineering Department, UCLA, 2024.

[2] Hartman E. P., Biermann D., Report No. 640, The Aerodynamic Characteristics of Full-Scale Propellers Having 2, 3, and 4 Blades of Clark Y and R. A. F. 6 Airfoil Sections, NACA, 1938

[3] McCormick, B. W., Aerodynamics, Aeronautics, and Flight Mechanics, Wiley, 1995.

[4] Pamadi, B. N., Performance, stability, dynamics, and control of airplanes, American Institute of Aeronautics and Astronautics, Inc., 2015.

[5] Raymer, D. P., Aircraft Design A Conceptual Approach, American Institute of Aeronautics and Astronautics, Inc., 1992.